

# Hair Cells Require Phosphatidylinositol 4,5-Bisphosphate for Mechanical Transduction and Adaptation

Moritoshi Hirono,<sup>1,3</sup> Charlotte S. Denis,<sup>1</sup>  
Guy P. Richardson,<sup>2</sup> and Peter G. Gillespie<sup>1,\*</sup>

<sup>1</sup>Oregon Hearing Research Center and  
Vollum Institute

Oregon Health and Science University  
3181 SW Sam Jackson Park Road  
Portland, Oregon 97239

<sup>2</sup>School of Life Sciences  
University of Sussex  
Falmer, Brighton BN1 9QG  
United Kingdom

## Summary

After opening in response to mechanical stimuli, hair cell transduction channels adapt with fast and slow mechanisms that each depend on  $\text{Ca}^{2+}$ . We demonstrate here that transduction and adaptation require phosphatidylinositol 4,5-bisphosphate ( $\text{PIP}_2$ ) for normal kinetics.  $\text{PIP}_2$  has a striking distribution in hair cells, being excluded from the basal region of hair bundles and apical surfaces of frog saccular hair cells. Localization of a phosphatidylinositol lipid phosphatase, Ptpqr, to these  $\text{PIP}_2$ -free domains suggests that Ptpqr maintains low  $\text{PIP}_2$  levels there. Depletion of  $\text{PIP}_2$  by inhibition of phosphatidylinositol 4-kinase or sequestration by aminoglycosides reduces the rates of fast and slow adaptation.  $\text{PIP}_2$  and other anionic phospholipids bind directly to the IQ domains of myosin-1c, the motor that mediates slow adaptation, permitting a strong interaction with membranes and likely regulating the motor's activity.  $\text{PIP}_2$  depletion also causes a loss in transduction current.  $\text{PIP}_2$  therefore plays an essential role in hair cell adaptation and transduction.

## Introduction

Hair cells are the inner ear's mechanical sensors: they respond electrically to external forces, like those imparted by a sound entering the hearing organ (the cochlea), or a head movement that activates the balance organs (the saccule, utricle, and semicircular canals). A hair cell accomplishes this mechanical to electrical transduction with its hair bundle, an asymmetric array of tens or hundreds of actin-filled stereocilia and, in many organs, the microtubule-based kinocilium. Excitatory (positive) movement of the hair bundle stretches a gating spring, which is either the filamentous link connecting adjacent stereocilia (the tip link) or is in series with this link (Assad et al., 1991; Kachar et al., 2000; Pickles et al., 1984). Tension in the stretched tip link biases a mechanically sensitive transduction channel toward its open state, admitting cations through the

channel that depolarize the hair cell. Two independent adaptation mechanisms allow the channel to close in the face of a sustained excitatory stimulus (Fettiplace and Ricci, 2003). Slow adaptation depends on myosin-1c (Myo1c), a molecular motor with an actin and ATP binding head, calmodulin binding IQ domains, and a phospholipid binding tail (Holt et al., 2002; Gillespie and Cyr, 2004). The force of the stimulus drags the myosin down a stereocilium, reducing tension in the gating spring and allowing the channels to close within tens of milliseconds. The rate of slow adaptation depends on  $\text{Ca}^{2+}$  entry through transduction channels (Assad and Corey, 1992), presumably by binding to calmodulin associated with Myo1c. Fast adaptation occurs when  $\text{Ca}^{2+}$  enters an open transduction channel and, by binding to a site on or near the channel, causes it to close within a few milliseconds or less (Wu et al., 1999).

Transmembrane proteins and membrane-associated proteins are often regulated by lipids. For example, polyphosphoinositides like phosphatidylinositol 4,5-bisphosphate ( $\text{PIP}_2$ ) modulate the activity of a wide array of ion channels and transporters (reviewed in Hilgemann et al., 2001). Many TRP channels, members of the family that is thought to encompass the transduction channel, are regulated by  $\text{PIP}_2$  and other lipids (Hilgemann et al., 2001). Moreover, the plasma membrane  $\text{Ca}^{2+}$ -ATPase (PMCA), the primary extruder of  $\text{Ca}^{2+}$  from hair bundles (Lumpkin and Hudspeth, 1998; Yamoah et al., 1998), is also regulated by  $\text{PIP}_2$  (Choquette et al., 1984). Little is known about the lipid composition of the stereocilia membrane, however, so the relevance of these observations to mechanotransduction is uncertain. In one notable exception,  $\text{PIP}_2$  was localized to hair bundles using a specific antibody (Tachibana et al., 1984), although its precise location and effect on mechanotransduction have hitherto not been investigated.

We report here that in frog saccular hair cells,  $\text{PIP}_2$  can be detected in basolateral membranes and the apical ends of hair bundles. The presence of the lipid phosphatase Ptpqr at bundle bases suggests that this phosphatase is responsible for maintaining low  $\text{PIP}_2$  levels there. By blocking the synthesis of  $\text{PIP}_2$  or sequestering it in the membrane, we show that  $\text{PIP}_2$  regulates the rates of fast and slow adaptation. We show here that a phospholipid binding domain is present in the IQ domains of Myo1c and propose that it underlies the sensitivity of slow adaptation to  $\text{PIP}_2$ .

## Results

### $\text{PIP}_2$ Is Localized in Hair Bundles

We sought to define the location of  $\text{PIP}_2$  more precisely using the large bundles of frog hair cells. We used a monoclonal antibody for  $\text{PIP}_2$  (2C11) that shows minimal cross-reactivity toward other phospholipids (Thomas et al., 1999). Phosphatidylinositol 3,4,5-trisphosphate ( $\text{PIP}_3$ ), the only other phospholipid for which this antibody has modest affinity, was not detectable in hair bundles with a  $\text{PIP}_3$ -selective antibody (data not shown). We were

\*Correspondence: gillespp@ohsu.edu

<sup>3</sup>Present address: Brain Science Institute, RIKEN, Wako 351-0198, Japan.

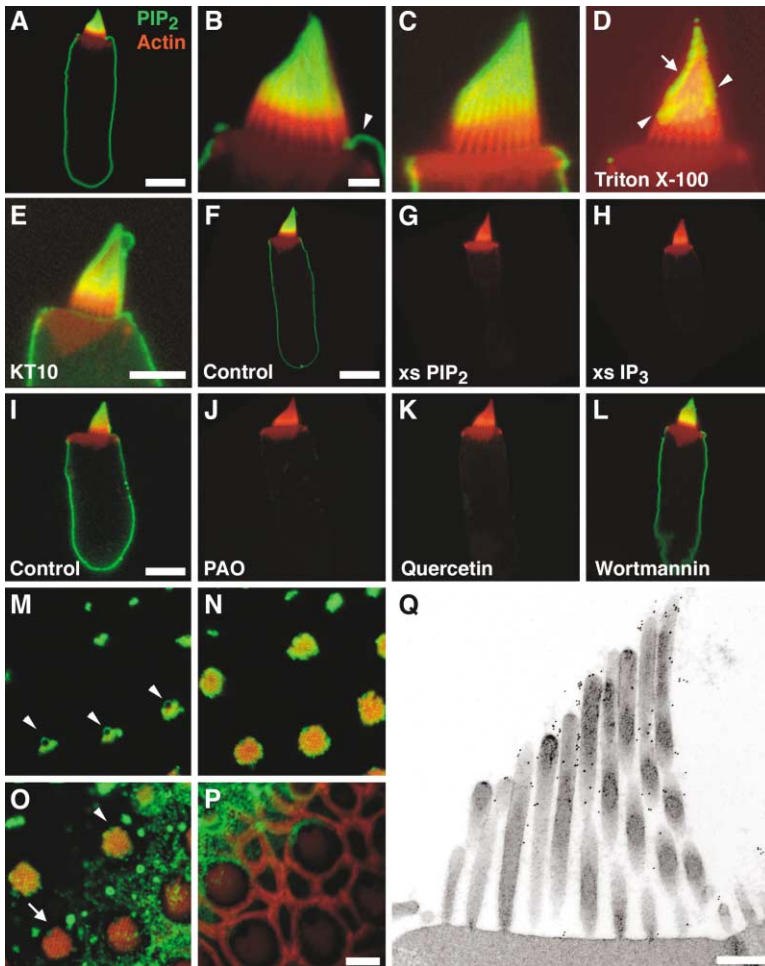


**Figure 1. PIP<sub>2</sub> Is Asymmetrically Distributed in Hair Cells**

(A–C) Three examples of PIP<sub>2</sub> immunoreactivity in isolated cells with fixative-saline permeabilization. Red, actin (detected with phalloidin); green, PIP<sub>2</sub> immunoreactivity with 2C11 antibody. Arrowhead in (B) indicates bridge of PIP<sub>2</sub> extending from basolateral surface to the base of the kinocilium. Scale bar in (A), 10 μm. Scale bar in (B) (2 μm) also applies to (C) and (D). (D) 1% Triton X-100 permeabilization on ice before fixation (2C11). (E) KT10 anti-PIP<sub>2</sub> antibody. Note complete staining of kinocilium and modest apical surface staining, occasionally seen with either antibody. Scale bar, 5 μm. (F) Control for (G) and (H) (2C11). Scale bar (5 μm) also applies to (G) and (H). (G) Coincubation with 40 μg/ml diC8-PIP<sub>2</sub> (2C11). (H) Coincubation with 40 μg/ml IP<sub>3</sub> (2C11). (I) Control for (J) and (K) (2C11). Scale bar (5 μm) also applies to (J)–(L). (J–L) Twenty minute preincubation with 100 μM PAO (J), 100 μM quercetin (K), or 50 μM wortmannin (L). 2C11 was used. (M–P) Whole-mount saccular epithelium, isolated without subtilisin treatment and labeled with 2C11. Confocal slices at 6 μm (M), 3.5 μm (N), 1.5 μm (O), and 0 μm (P) from the base of leftmost bundle. Arrowheads in (M) indicate kinociliary bulbs near the top of the bundle. In (O), note PIP<sub>2</sub> immunoreactivity in bundle at elevated level (arrowhead), but little PIP<sub>2</sub> in bundle at a lower level (arrow). Scale bar, 5 μm. (Q) Immunogold electron microscopy of hair cell in intact saccular epithelium using 2C11, without subtilisin treatment and with fixative-saline permeabilization. Scale bar, 500 nm.

also unable to detect the immediate precursor to PIP<sub>2</sub>, phosphatidylinositol 4-phosphate [PI(4)P], using a specific antibody (data not shown), presumably because it is so rapidly converted to PIP<sub>2</sub>.

The distribution of PIP<sub>2</sub> in isolated hair cells was remarkable (Figures 1A–1C). PIP<sub>2</sub> was evenly distributed throughout the hair cell's basolateral membrane, yet was nearly completely absent from the cell's apical surface and the taper region of the stereocilia. PIP<sub>2</sub> was present in stereocilia, but only above the ankle link region, which extends ~1 μm above the tapers. The entire kinocilium was labeled with anti-PIP<sub>2</sub> antibodies (Figure 1E), as was a small bridge of apical surface membrane between the base of the kinocilium and the basolateral surface of the hair cell (Figure 1B, arrowhead). Another anti-PIP<sub>2</sub> antibody, KT10 (Fukami et al., 1988), produced very similar results to those with 2C11 (Figure 1E).

Several control experiments established that immunocytochemistry with 2C11 specifically detected PIP<sub>2</sub> in hair cells. Coincubation of the anti-PIP<sub>2</sub> antibody with >1000-fold molar excess of diC8-PIP<sub>2</sub>, a PIP<sub>2</sub> with eight-carbon acyl chains, or IP<sub>3</sub>, the head group of PIP<sub>2</sub>, eliminated antibody labeling (Figures 1F–1H). Phenylarsine oxide (PAO) and quercetin inhibit all isoforms of phosphatidylinositol 4-kinase (PI4K), which catalyzes the first step in synthesis of PIP<sub>2</sub> from phosphatidylinositol (Wiedemann et al., 1996; Cochet and Chambaz, 1986); both

reagents rapidly deplete PIP<sub>2</sub> from cells (Varnai and Balla, 1998). Although PAO and quercetin each inhibit a variety of enzymes, their inhibitory spectra apparently only overlap with PI4K. PAO and quercetin reduced PIP<sub>2</sub> immunoreactivity in hair cells to undetectable levels (Figures 1I–1K). Treatment with 30 μM PAO for 6 min was sufficient to eliminate immunoreactivity. These results suggest that hair cells have a robust polyphosphoinositide flux, as reduction of PIP<sub>2</sub> levels by synthesis inhibitors relies on active phospholipases or lipid phosphatases. PAO and quercetin were not universally effective; PIP<sub>2</sub> remained at near-control levels in the stereocilia of a fraction of hair cells (20%), most often those with narrow cell bodies and bundles. Wortmannin, which at low micromolar concentrations can inhibit type III PI4K (Balla, 1998), did not deplete PIP<sub>2</sub>, even at 50 μM (Figure 1L); this result suggested that hair bundles contain type II PI4K, the other common isoform.

PIP<sub>2</sub> immunoreactivity was most prominent when hair cells were not treated with detergents. Under our fixation conditions, successful phalloidin labeling demonstrated that hair cells were indeed permeabilized; formaldehyde fixation with saline solutions can permeabilize cells, perhaps through osmotic disruption (Hinnert et al., 1999; Hannah et al., 1998). Our ability to detect PIP<sub>2</sub> was also aided by transbilayer scrambling of membrane lipids (Williamson and Schlegel, 1994), which partially exposes

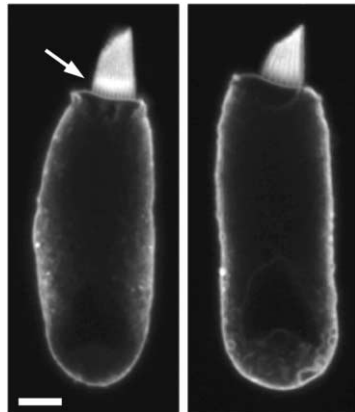


**Figure 2. Localization of PS in Hair Cells**  
Two examples of annexin V labeling of fixed isolated hair cells, permeabilized with saponin. Note band of annexin V labeling at ankle link region found in some cells (arrow). Scale bar, 5  $\mu$ m.

PIP<sub>2</sub> and phosphatidylserine (PS) on the extracellular surface following dissection of hair cell epithelia (M.H. and P.G.G., unpublished data). The anti-PIP<sub>2</sub> antibody therefore detected PIP<sub>2</sub> in both the extracellular and intracellular leaflets.

A different pattern of PIP<sub>2</sub> distribution was seen when the cell was subjected to more extensive detergent permeabilization. Although detergents generally solubilize membrane lipids, some lipids—such as those in classically defined lipid rafts (Edidin, 2003)—resist extraction by Triton X-100 at 4°C. We found that PIP<sub>2</sub> at stereocilia tips resisted cold Triton extraction, as did a fraction of the PIP<sub>2</sub> above the ankle link region (Figure 1D). Thus, although most of the PIP<sub>2</sub> in the stereocilia was readily extracted with detergent, specific populations were sequestered in detergent-resistant pools.

Restriction of PIP<sub>2</sub> to the apical end of hair bundles was also seen in saccular epithelial preparations (Figures 1M–1P), indicating that basal PIP<sub>2</sub> exclusion was not an artifact of cell isolation. Moreover, immunogold electron microscopy of whole saccular epithelia confirmed that PIP<sub>2</sub> immunoreactivity was primarily restricted to the apical halves of bundles (Figure 1Q).

### PS Is Present in Hair Bundles

PS is the predominant anionic phospholipid in the intracellular leaflet of the plasma membrane. We used fluorescently labeled annexin V, which binds PS with high affinity (Gerke and Moss, 2002), to localize PS in hair cells. We found robust annexin V labeling in the basolateral membrane, the apical surface, and the stereocilia (Figure 2). In some cells, PS was concentrated in stereocilia in a band at the position of the ankle links, in the approximate location where PIP<sub>2</sub> is absent (e.g., Figure 2, left). Saponin treatment substantially increased the annexin V signal (data not shown), suggesting that most PS was on the intracellular leaflet of the stereocilia membrane.

### Ptprq Lipid Phosphatase May Maintain PIP<sub>2</sub>-free Zones

The hair cell antigen, a 275 kDa hair bundle protein recently shown to be the phosphatidylinositol lipid phos-

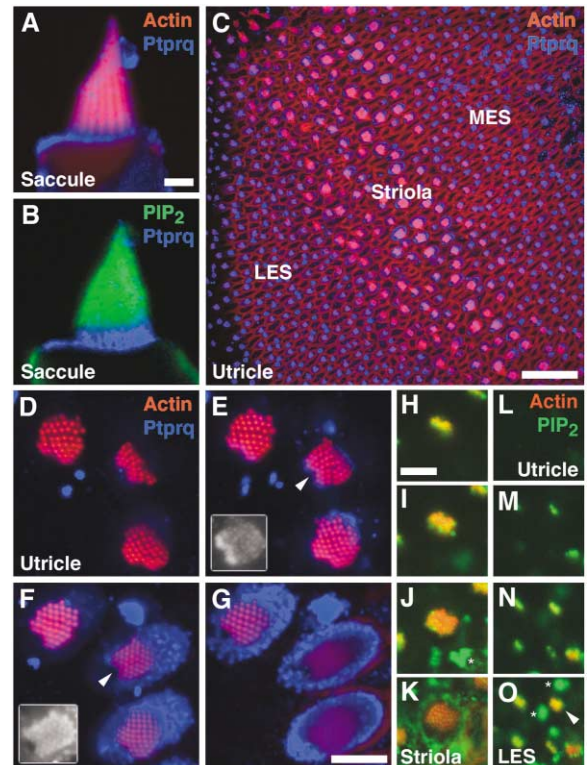


**Figure 3. Reciprocal Distribution of PIP<sub>2</sub> and Lipid Phosphatase Ptprq**

(A) Ptprq in isolated frog saccular hair cell. Red, actin; blue, Ptprq. Scale bar (2  $\mu$ m) also applies to (B). (B) Inverse correspondence of Ptprq and PIP<sub>2</sub> in saccule hair cell. Green, PIP<sub>2</sub>; blue, Ptprq. Ptprq labeling near stereocilia tips is probably in membrane blebs, not in the kinocilium; Ptprq was never observed in kinocilia in whole mounts (e.g., [C]). (C) Ptprq is basally located only in striolar hair cells of the frog utricle. Projection of confocal stack through hair bundles and apical surfaces. Scale bar, 25  $\mu$ m. (D–G) Ptprq in utricular hair bundles in the striola; confocal slices at 6  $\mu$ m (D), 2  $\mu$ m (E), 1  $\mu$ m (F), and 0  $\mu$ m (G) from the base of the middle bundle. Note extended Ptprq staining in the tallest row of stereocilia ([E], inset). Insets in (E) and (F) are grayscale images of bundles indicated by arrowheads. Scale bar in (G) (5  $\mu$ m) also applies to (D)–(F). (H–O) PIP<sub>2</sub> in striolar (H–K) and extrastriolar (L–O) utricular hair bundles; confocal slices at 6  $\mu$ m (H and L), 4  $\mu$ m (I and M), 2  $\mu$ m (J and N), and 0  $\mu$ m (K and O) from bundle base. Arrowhead in (O) indicates extrastriolar hair bundle. Asterisks in (J) and (O) indicate bright PIP<sub>2</sub> immunoreactivity at epithelial surface, which may be shed membrane. Scale bar in (H) (5  $\mu$ m) also applies to (I)–(O).

phatase Ptprq, is basally restricted in some hair bundles (Goodyear et al., 2003). Because the location of PIP<sub>2</sub> appeared to be inversely correlated with Ptprq, we used antibodies to localize this phosphatase. Ptprq was concentrated on the apical surface and taper region of frog saccule hair cells (Figure 3A); in double-labeling experiments, we found a near-perfect reciprocal correspondence between PIP<sub>2</sub> and Ptprq (Figure 3B). Because Ptprq efficiently hydrolyzes PIP<sub>2</sub> (Oganesian et al., 2003), this lipid phosphatase may be responsible for low PIP<sub>2</sub> levels in hair cell apical surfaces and in the lower regions of hair bundles.

We also examined Ptprq distribution in hair cells of the frog utricle. Similar to its distribution in other vestibular organs (Goodyear and Richardson, 1992), Ptprq was

basally restricted only within hair cells in the central striolar region of the utricular macula (Figures 3C–3G); by contrast, Ptpqrq was distributed throughout stereocilia of extrastriolar hair cells (Figure 3C). We also noted that Ptpqrq extended more distally toward the tips of the ~4 tallest stereocilia of striolar hair cells (Figure 3E).

As in saccular epithelium preparations, we found that PIP<sub>2</sub> immunoreactivity was concentrated apically in striolar hair cells of the frog utricle (Figures 3H–3K). Surprisingly, despite high levels of Ptpqrq, extrastriolar hair cells had substantial levels of PIP<sub>2</sub> immunoreactivity throughout their bundles (Figures 3L–3O).

### Inhibitors of PIP<sub>2</sub> Synthesis Reduce Fast and Slow Adaptation Rates

To determine whether PIP<sub>2</sub> plays a role in transduction and adaptation, we treated hair cells with reagents that deplete PIP<sub>2</sub>. We dissociated frog saccule hair cells and mechanically stimulated their hair bundles, measuring transduction currents and adaptation with whole-cell voltage-clamp recording (Figure 4).

We inhibited PI4K with PAO in six cells and found that, in all cases, PIP<sub>2</sub> depletion reduced the rate of adaptation (Figure 4B). In frog hair cells, a stimulus that increases a transduction channel's open probability ( $P_o$ ) to ~0.5 leads to subsequent channel closure that is dominated by fast adaptation;  $\tau_{0.5}$  is the time constant that describes the relaxation of transduction current for such a stimulus. In cells treated with 30  $\mu$ M PAO,  $\tau_{0.5}$  increased 3-fold (Figure 4J). Resting  $P_o$  is thought to be set by the balance between climbing and slipping adaptation set by the slow-adaptation motor (Assad and Corey, 1992); 30  $\mu$ M PAO also increased resting  $P_o$  3-fold (Figure 4K). Transduction currents disappeared slowly with 30  $\mu$ M PAO ( $\tau = 15$  min for a single exponential fit; data not shown); at higher concentrations, loss of transduction was much faster (100  $\mu$ M,  $\tau = 7.1$  min; 200  $\mu$ M,  $\tau = 1.8$  min; Figure 4I).

All effects of PAO were blocked completely by coinubation with dithiothreitol (DTT) (Figure 4C), which forms an inactive complex with PAO (Schaefer et al., 1994). By contrast, the effects of 30  $\mu$ M PAO on  $\tau_{0.5}$  were not prevented by inclusion of 200  $\mu$ M diC8-PIP<sub>2</sub> in the recording electrode (Figure 4D). This short-chain PIP<sub>2</sub> does not integrate substantially into membranes, however, and cannot modulate some PIP<sub>2</sub>-dependent proteins (Rohacs et al., 1999). Although PIP<sub>2</sub> derivatives with longer acyl chains might have reversed PAO's effects, they are expected to form vesicles that transfer poorly from the recording electrode into the cell and from the cell body into the bundle; in addition, attempts to deliver long-chain PIP<sub>2</sub> derivatives with PIP shuttles (Ozaki et al., 2000) were unsuccessful. diC8-PIP<sub>2</sub> did effectively prevent the increase in resting  $P_o$  exerted by PAO (Figure 4K), suggesting that modulation of slow adaptation does not require long PIP<sub>2</sub> acyl chains. In addition, diC8-PIP<sub>2</sub> partially prevented the loss in transduction current elicited by 30  $\mu$ M PAO ( $\tau = 32$  min; data not shown). By itself, 200  $\mu$ M diC8-PIP<sub>2</sub> had small, statistically insignificant effects on  $\tau_{0.5}$  and resting  $P_o$  (data not shown). diC4-PIP<sub>2</sub> had effects similar to those of diC8-PIP<sub>2</sub> (data not shown).

We also used a double-stimulus protocol (Eatock et

al., 1987) to confirm the effect of PAO on adaptation. Sliding of the I(X) relation along the displacement axis, a direct measure of adaptation, was reduced substantially by PAO (data not shown); a 500 nm displacement induced a shift of  $429 \pm 15$  nm before and  $145 \pm 71$  nm after PAO treatment ( $n = 3$ ).

Quercetin, which also inhibits PI4K, produced effects on adaptation that were nearly identical to those seen with PAO (6/6 cells; Figures 4F, 4J, and 4K). Quercetin also reduced transduction current amplitudes, although to a lesser extent than PAO ( $\tau = 39$  min; data not shown). By contrast, 30–50  $\mu$ M wortmannin, which did not affect stereocilia PIP<sub>2</sub> levels (Figure 1), also did not affect transduction or adaptation (3/3 cells; Figure 4E). Even hair cells that had been pretreated with 50  $\mu$ M wortmannin for 15 min prior to whole-cell recording still had rapid adaptation (data not shown), confirming the drug's lack of effect.

By binding to and sequestering PIP<sub>2</sub>, millimolar concentrations of aminoglycosides like neomycin and gentamicin can inhibit PIP<sub>2</sub>-dependent processes (Wang et al., 1984). Although extracellular aminoglycosides block transduction channels, they are ineffective at channel block when introduced into the cytoplasm of a cell (Kroese et al., 1989). Intracellular aminoglycosides caused many hair cells to swell, making their effects on adaptation difficult to interpret due to mechanical artifacts. In recordings that were mechanically stable, gentamicin (Figures 4G, 4J, and 4K) and neomycin (data not shown) slowed adaptation upon intracellular dialysis; at 1 mM, this effect was more pronounced for gentamicin than neomycin.

Many cells regulate PIP<sub>2</sub> levels in response to external stimuli using transmembrane receptors, G proteins, and phospholipase C $\beta$ . Agents that activate (GTP $\gamma$ S; 10–100  $\mu$ M) or inhibit (GDP $\beta$ S; 3 mM) this pathway had no statistically significant effect on  $\tau_{0.5}$  or resting  $P_o$  (data not shown), however, suggesting that phospholipase C $\beta$  does not participate in regulation of transduction or adaptation.

In other experiments, dialysis of hair cells with IgG or IgM anti-PIP<sub>2</sub> antibodies failed to produce changes in adaptation rate (data not shown). These results were not surprising, however, because the large antibody sizes (150 and 900 kDa) must prevent rapid entry into the cell and access to the hair bundle.

### Dissection of Effects of PAO on Fast and Slow Adaptation

To more accurately extract the individual contributions of fast and slow adaptation, we used the inferred shift method to dissect transduction current records (Shepherd and Corey, 1994). With the assumption that both fast and slow adaptation are described by independent exponential shifts of the I(X) curve along the displacement axis, without changes in the curve's shape or amplitude, this method allows extraction of the underlying change in hair cell sensitivity that is otherwise distorted by the nonlinear transduction current. We determined the extent of adaptation ( $X_e$ ) at each time point, producing an  $X_e(t)$  plot for each stimulus amplitude (Figures 5A and 5B). We globally fit each set of  $X_e(t)$  relations with two amplitudes per stimulus but only two exponential

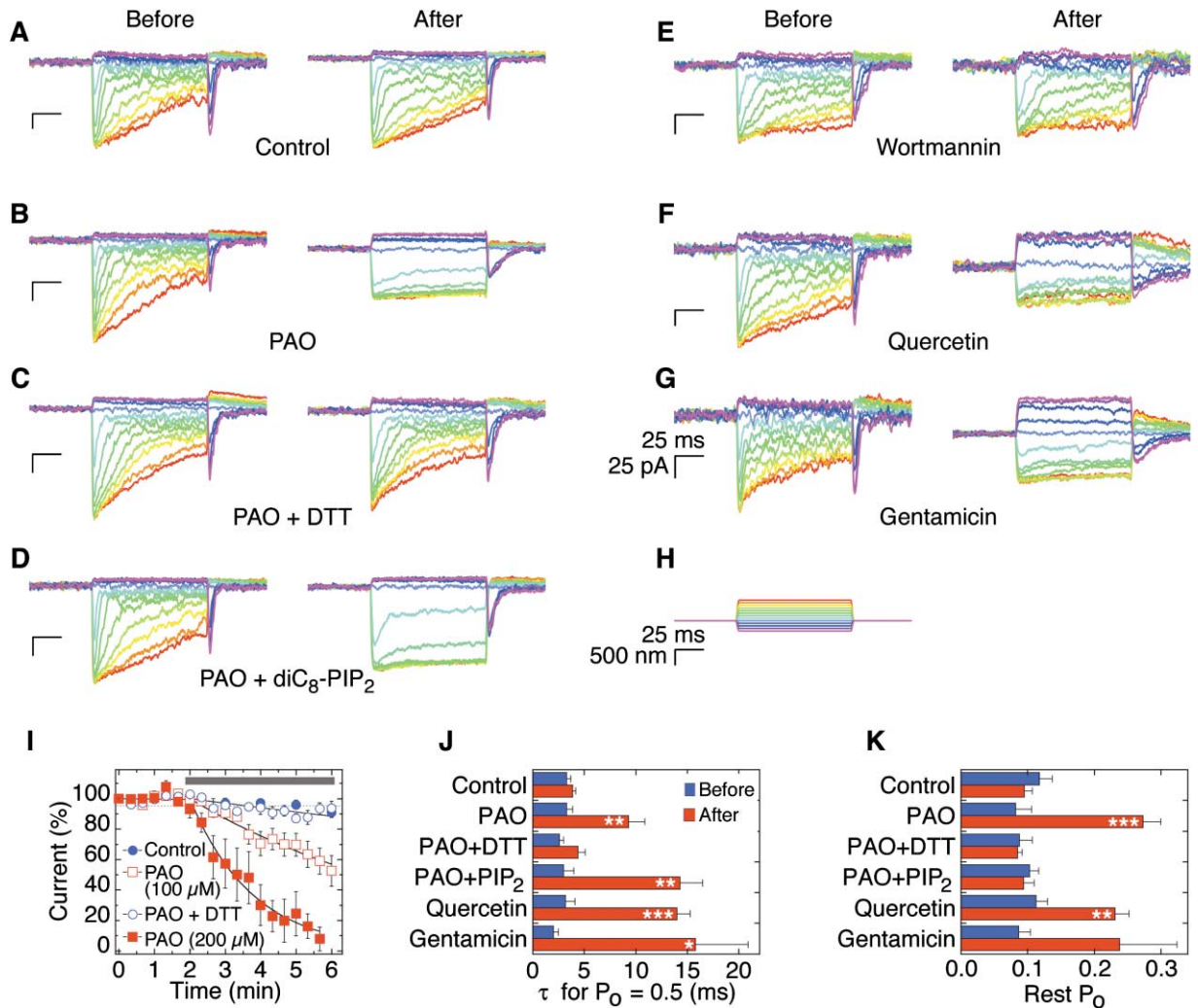


Figure 4. Inhibitors of PIP<sub>2</sub> Slow Adaptation and Block Transduction

(A) Dialysis with control solution (2.5 min and 10.5 min after break-in).

(B) PAO (30  $\mu$ M) slows adaptation (right, 5 min after PAO application).

(C) DTT (3 mM) prevents the effects of 100  $\mu$ M PAO (right, 4 min after PAO application). PAO and DTT were applied simultaneously.

(D) diC<sub>8</sub>-PIP<sub>2</sub> (200  $\mu$ M) in the recording electrode does not reverse the effects of 30  $\mu$ M PAO (right, 4 min after PAO application).

(E) Wortmannin (50  $\mu$ M) does not affect adaptation (right, 11 min after application).

(F) Quercetin (100  $\mu$ M) slows adaptation (right, 6 min after application).

(G) Gentamicin (1 mM) slows adaptation (right, 7.5 min after break-in). Scale bars for (A)–(G) are all 25 pA and 25 ms.

(H) Stimuli used for (A)–(G).

(I) Transduction current amplitude in response to PAO application. PAO (100  $\mu$ M or 200  $\mu$ M) was applied during the time indicated by the gray bar. In some experiments, DTT (3 mM) was included to block the effects of 100  $\mu$ M PAO.

(J) Time constants for exponential fits to transduction currents in response to stimuli eliciting  $P_o \approx 0.5$ . Significance is indicated as \* $p < 0.05$ , \*\* $p < 0.01$ , and \*\*\* $p < 0.001$ .

(K) Transduction channel resting open probability. Significance indicated as in (J).

time constants for the entire data set, one for fast adaptation and one for slow. This analysis fit the data well and clearly distinguished fast and slow adaptation. Our average fast adaptation time constant (2 ms) was slightly slower than those measured by others using the same preparation (Vollrath and Eatock, 2003), presumably because of our relatively slow mechanical stimulator; slow adaptation time constants (20 ms) were similar to those reported elsewhere. Adaptation rates were relatively stable during dialysis lasting 5 min or more; in four control hair cells, the rate of fast adaptation diminished by

only 30%, while the rate of slow adaptation remained unchanged.

Although all PAO-treated cells had substantially reduced fast and slow adaptation as assessed by eye, current records were in some cases too noisy to use the inferred shift method. We were successful in extracting fast and slow rates, however, from transduction currents of three cells that had been treated with 30  $\mu$ M PAO for 4–8 min. In these cells, PAO reduced the extent of adaptation (fast and slow combined) from 91% to 64% (Figure 5C). PAO inhibited both fast and slow adap-

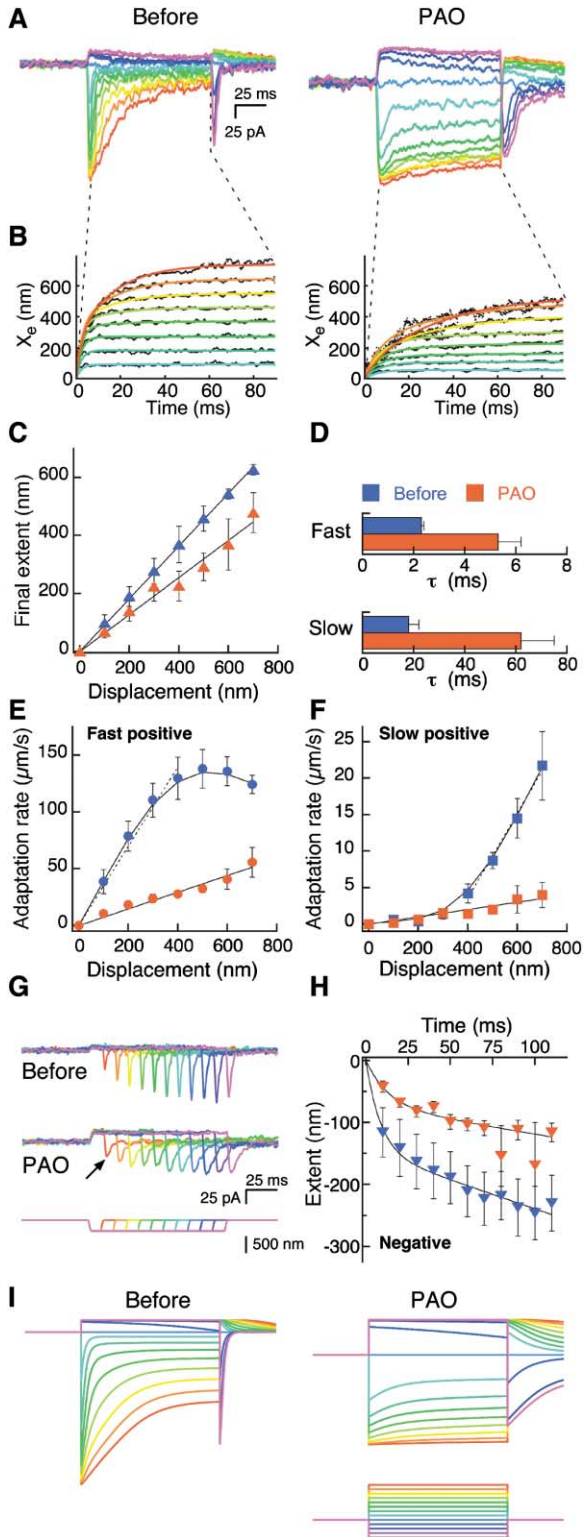


**Figure 5. Phenylarsine Oxide Reduces Rates of Fast and Slow Adaptation**

(A) Transduction currents before and ~6 min after application of 30  $\mu$ M PAO. Displacements were identical to those in Figure 4H. (B) Adaptive shifts ( $X_e$ ) calculated from data in (A). Double-exponential fits use the same coloring scheme as currents in (A). (C) Extent of adaptation. Calculated from summed fast and slow  $X_e$  values. Blue symbols, before PAO treatment; red symbols, after. (D) Time constants for adaptation. Calculated from fits to  $X_e$  plots. (E) Dependence of fast adaptation rates on positive displacement size. The fast adaptation rate constant was determined by fitting the 100–400 nm control points (dashed line) or all PAO points. Blue symbols, before PAO treatment; red symbols, after. (F) Slow adaptation. The slow adaptation rate constant was determined by fitting the 400–700 nm control points (dashed line) or all PAO points. Blue symbols, before PAO treatment; red symbols, after. (G) Transduction currents during and after negative deflections. Note overshoots reflecting amount of adaptation (arrow). (H) Extent of adaptation to inhibitory deflections. Data were fit with sum of exponential and linear components; fits were weighted by errors. Blue symbols, before PAO treatment; red symbols, after. (I) Simulated transduction currents before and after PAO treatment. Adaptation was modeled similarly to that described in Shepherd and Corey (1994) with the addition of fast adaptation. Parameter values used are from Table 1.

tation to positive deflections. The time constant for fast adaptation increased from  $2.3 \pm 0.1$  ms to  $5.3 \pm 0.9$  ms, while the time constant for slow adaptation increased from  $18 \pm 4$  ms to  $62 \pm 13$  ms (Figure 5D). Rate constants for adaptation to positive stimuli ( $S_{fast}$  and  $S_{slow}$ ) were determined from the slope of the displacement adaptation rate curve in the relevant displacement range. Prior to PAO,  $S_{fast}$  was  $350$  s $^{-1}$  in response to displacements of 100–400 nm; PAO treatment reduced it 5-fold to  $73$  s $^{-1}$  (Figure 5E). Before PAO treatment,  $S_{slow}$  was  $58$  s $^{-1}$  in response to displacements of 400–800 nm; it was reduced 10-fold to only  $5$  s $^{-1}$  after PAO treatment (Figure 5F). Slow and fast adaptation rates continued to decrease during continued exposure to PAO.

To determine the effect of PAO on  $C_{slow}$ , the rate of adaptation motor climbing, we deflected bundles with saturating inhibitory displacements for 10–110 ms (Figure 5G), then determined the shift of the  $I(X)$  curve required to produce the overshoot currents that appeared when the bundle was returned to its resting position (Holt et al., 2002). Adaptation to large inhibitory deflections was fit well with a sum of an exponential and a linear component (data not shown and Figure 5H). We assumed that the exponential component resulted from unbinding of  $Ca^{2+}$  from the fast adaptation sensor and reversal of fast channel closure; the initial rate was  $-17.5$   $\mu$ m s $^{-1}$  before and  $-5.8$   $\mu$ m s $^{-1}$  after PAO treatment. The rate of the linear component, which we assumed to represent motor climbing, was decreased by PAO from  $-0.95$   $\mu$ m s $^{-1}$  to  $-0.52$   $\mu$ m s $^{-1}$ .

To determine how  $PIP_2$  regulates adaptation, we used values determined for the slipping rate constant, climbing rate, and extent of adaptation (Table 1) to simulate transduction currents in the presence of fast and slow adaptation (Figure 5I). Our model replicated most of the features of the transduction current records before and after PAO treatment (compare to Figures 4B and 5A). For example, the model predicts that the resting  $P_o$  of the modeled currents increases from 0.07 to 0.28, similar to the 0.08 to 0.24 increase that was experimentally observed (Figure 4K).

### **IQ Domains of Myo1c Bind to Anionic Phospholipids**

The effects of  $PIP_2$  depletion on slow adaptation suggested that this lipid could affect Myo1c mechanics or

Table 1. Parameter Values for Fast and Slow Adaptation

Parameter	Before	PAO
Gating spring stiffness ( $K_g$ ) <sup>a</sup>	538 $\mu\text{N m}^{-1}$	538 $\mu\text{N m}^{-1}$
Adaptation extent ( $X_{\text{set(-)}}$ ) <sup>b</sup>	91%	64%
Extent spring stiffness ( $K_e$ ) <sup>c</sup>	53 $\mu\text{N m}^{-1}$	303 $\mu\text{N m}^{-1}$
Slow slipping time constant ( $\tau_{\text{slow}}$ ) <sup>b</sup>	18 ms	62 ms
Slow slipping rate ( $S_{\text{slow}}$ ) <sup>d</sup>	58 $\text{s}^{-1}$	5 $\text{s}^{-1}$
Slow adaptation frictional coefficient ( $Z$ ) <sup>e</sup>	12 $\mu\text{N s m}^{-1}$	52 $\mu\text{N s m}^{-1}$
Adaptation motor climbing rate ( $C_{\text{slow}}$ ) <sup>f</sup>	3.7 $\mu\text{m s}^{-1}$	2.5 $\mu\text{m s}^{-1}$
Adaptation motor force production ( $F_m$ ) <sup>g</sup>	43 pN	130 pN
Fast adaptation time constant ( $\tau_{\text{fast}}$ ) <sup>b</sup>	2.3 ms	5.3 ms
Fast slipping rate ( $S_{\text{fast}}$ ) <sup>d</sup>	350 $\text{s}^{-1}$	73 $\text{s}^{-1}$

The above values are referenced to the tip of the bundle; the geometrical gain  $\gamma$  ( $=0.14$ ) can be used to convert these values to those applying at the level of an individual adaptation motor complex (Gillespie and Cyr, 2004).

<sup>a</sup> From Shepherd and Corey (1994).

<sup>b</sup> Measured.

<sup>c</sup> Calculated from  $K_e = K_g [(1 - X_{\text{set(-)}})/X_{\text{set(-)}}]$ .

<sup>d</sup> Measured from displacement rate plot.

<sup>e</sup> Calculated from  $\tau (K_g + K_e)$ .

<sup>f</sup> Measured from initial slope of slow component.

<sup>g</sup> Calculated from  $Z C_{\text{slow}}$ .

activity. Although the basic tail of Myo1c should bind to PIP<sub>2</sub>, Tang et al. (2002) also showed that transient Ca<sup>2+</sup> treatment dramatically decreased the dissociation of Myo1c from phospholipid vesicles containing PS, implying that Ca<sup>2+</sup> exposes an additional anionic lipid binding domain of Myo1c. We sought to detect this second binding site in frog Myo1c and to determine whether PIP<sub>2</sub> could also bind to it.

We found that a fragment of frog Myo1c containing all four IQ domains and the tail (T701; see Figure 6A) sedimented with PS vesicles only in the presence of Ca<sup>2+</sup> (Figure 6B). Moreover, over a broad range of Ca<sup>2+</sup> concentrations, when Myo1c was mixed with PS vesicles, one to two calmodulins per Myo1c dissociated (Figure 6C), similar to results with Myo1a (Swanlung-Collins and Collins, 1992). Although Ca<sup>2+</sup> also dissociated calmodulin from Myo1c in the absence of PS vesicles (Figure 6C), as shown previously (Zhu et al., 1996; Gillespie and Cyr, 2002), much higher concentrations of the ion were required. The apparent reciprocal binding of calmodulin and phospholipids to Myo1c led us to examine whether IQ domains were involved; IQ2 and IQ3, in particular, contain clusters of basic residues, which often make up binding sites for anionic lipids (Lemmon, 2003).

To qualitatively measure phospholipid binding, we used Myo1c to probe phospholipids bound to nitrocellulose membranes ("PIP strips"). In the presence of Ca<sup>2+</sup>, several Myo1c constructs bound to a variety of negatively charged lipids, including PS and PIP<sub>2</sub> (Figure 6D). N123, which only has three IQ domains and lacks the lipid binding tail, bound as well as the other constructs.

Although useful for an initial screen of binding selectivity, the orientation of phospholipids on PIP strips may not resemble that found in real membranes. To avoid this limitation, we used a solid-phase phospholipid binding assay (Fukami et al., 1996) to measure binding of phospholipid vesicles to immobilized N123. We confirmed that N123 bound to PS- and PIP<sub>2</sub>-containing vesicles (Figure 6E), noting that binding to PS or PIP<sub>2</sub> was reduced by calmodulin in the presence of either Ca<sup>2+</sup> or

EGTA. In the presence of EGTA, calmodulin competed with vesicles for binding to N123; calmodulin was more potent in competing with PS vesicles than with PIP<sub>2</sub> vesicles (Figure 6F), consistent with the suggestion that the N123-PIP<sub>2</sub> interaction was stronger than N123-PS. Taken together, these data show that Myo1c can bind anionic phospholipids, notably PIP<sub>2</sub>, using lipid binding domains in the tail and IQ domains. In order for exposure of the IQ domain lipid binding domain, however, one to two calmodulins must dissociate.

## Discussion

Our results suggest that polyphosphoinositide lipids control gating of transduction channels in hair cells through several distinct mechanisms. First, high concentrations of PI4K inhibitors eradicate mechanotransduction, suggesting that transduction channels require polyphosphoinositides for gating or that the transduction complex depends on polyphosphoinositides for structural integrity. Second, polyphosphoinositides strongly affect the rate of slipping adaptation (and more modestly affect climbing adaptation) by the slow-adaptation motor, probably because of direct interaction of lipids with Myo1c. Finally, the rate of rapid Ca<sup>2+</sup>-dependent closure of transduction channels, fast adaptation, depends on polyphosphoinositide levels. Because inhibition of PI4K should reduce both PIP<sub>2</sub> and PI(4)P levels, the effects of PAO and quercetin might be due to depletion of PI(4)P instead of PIP<sub>2</sub>. We doubt that PI(4)P is the important lipid, however; in other cell types, PI(4)P is rapidly phosphorylated to PIP<sub>2</sub> in the plasma membrane, so that PI(4)P levels are typically more than 10-fold lower than those of PIP<sub>2</sub> (Augert et al., 1989). Consistent with those observations, we did not detect PI(4)P in stereocilia membranes using conditions giving prominent PIP<sub>2</sub> immunoreactivity. Although Myo1c also bound to several phosphatidylinositol 3-phosphates (Figure 6D), we do not believe that these polyphosphoinositides affect adaptation; wortmannin, a highly potent phosphatidylinositol 3-kinase inhibitor (Arcaro and Wymann, 1993), did

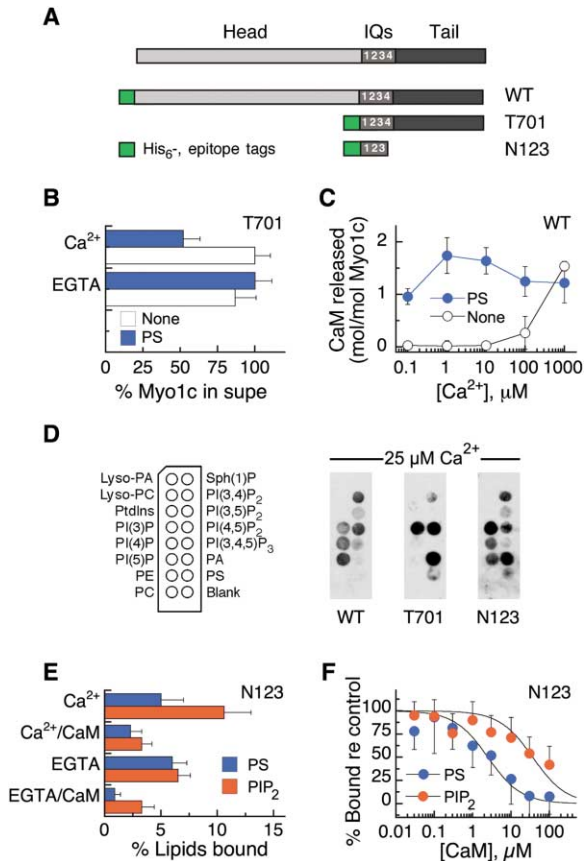


**Figure 6.** Myo1c Binds to Anionic Phospholipids with Its IQ Domains (A) Structure of Myo1c constructs used. T701 includes amino acids 701–1028, while N123 includes amino acids 701–790. (B)  $\text{Ca}^{2+}$  dependence of Myo1c (T701) sedimentation in the presence (PS) or absence (None) of 100 mol% PS vesicles. Myo1c levels were detected by ELISA. (C)  $\text{Ca}^{2+}$  dependence of calmodulin release from Myo1c (WT) in the presence (PS) or absence (None) of 100 mol% PS vesicles. Calmodulin levels were detected by ELISA. (D) Myo1c constructs bound to anionic phospholipids on PIP strips in the presence of  $\text{Ca}^{2+}$ . Bound Myo1c detected by immunoblotting. (E) Binding of 50 mol% PS or  $\text{PIP}_2$  vesicles to immobilized N123. Vesicles also contained 40 mol% PC and 10 mol% rhodamine-PE. Averaged data ( $\pm$  SEM) from five experiments. (F) Competition for binding of 50 mol% PS or 50 mol%  $\text{PIP}_2$  vesicles to immobilized N123 by soluble calmodulin (in the presence of EGTA). Fit with  $100 \times [1 - \text{CaM}/(\text{CaM} + \text{IC50})]$ , where CaM is the calmodulin concentration.

not affect transduction or adaptation (Figure 4E). We therefore conclude that  $\text{PIP}_2$ —and not other polyphosphoinositides—plays an important role in controlling transduction channel gating in hair cells.

#### **$\text{PIP}_2$ Is Asymmetrically Distributed in Hair Cells**

As detected with antibodies,  $\text{PIP}_2$  has a surprising distribution in hair cells, being excluded from the apical surface and lower part of the stereocilia.  $\text{PIP}_2$  is usually detected by transfecting cells with plasmids that direct expression of GFP-tagged pleckstrin homology (PH) domains (Varnai and Balla, 1998). Our inability to transfect hair cells prevented us from exploiting this strategy, which also has its limitations; PH domains bind relatively

weakly to  $\text{PIP}_2$  and may only recognize  $\text{PIP}_2$  in the context of specific membrane proteins that might not be present in stereocilia (Balla et al., 2000). By contrast, anti- $\text{PIP}_2$  antibodies have been shown to efficiently and selectively recognize  $\text{PIP}_2$  (Fukami et al., 1988; Tachibana et al., 1984; Thomas et al., 1999), including  $\text{PIP}_2$  present in hair bundles (Tachibana et al., 1984). In our case, immunolocalization of the lipid phosphatase Ptpqr in domains where  $\text{PIP}_2$  was absent further reinforced the  $\text{PIP}_2$  localization that we show. This distribution raises at least two questions: first, how are the  $\text{PIP}_2$ -free domains maintained, and second, what is their functional relevance?

Given their reciprocal localization, Ptpqr is the best candidate to maintain the  $\text{PIP}_2$ -free domains near stereocilia insertions. Ptpqr is required for auditory function (Goodyear et al., 2003); mouse auditory hair bundles that lack Ptpqr become disorganized shortly after birth, leading to eventual hair cell degeneration. Perhaps the presence of  $\text{PIP}_2$  in this location is detrimental to stereocilia integrity; the presence of  $\text{PIP}_2$  at stereocilia insertions, where membrane curvature is particularly acute, might prevent proper membrane anchoring or dynamics.

Another significant role for maintaining  $\text{PIP}_2$  domains in stereocilia may be in controlling turnover of stereocilia actin filaments (Rzadzinska et al., 2004). Although control of polymerization of parallel actin bundles, like those in stereocilia, is poorly understood,  $\text{PIP}_2$  plays a well-established role in regulation of polymerization of branched actin networks (Yin and Janmey, 2003). It is striking that  $\text{PIP}_2$  is present in a detergent-resistant pool at stereocilia tips, where actin filaments are polymerized, and is excluded from stereocilia tapers, where actin filaments must be continuously depolymerized at the membrane. Nevertheless, because mature stereocilia elongate at  $<4$  nm/min (Rzadzinska et al., 2004), it is unlikely that the PI4K inhibitor effects that we saw were due to actin filament disruption.

#### **Anionic Phospholipids Contribute to the Adaptation Motor Complex**

Because rapid  $\text{PIP}_2$  turnover in hair bundles will be energetically costly,  $\text{PIP}_2$  likely plays a role in stereocilia that justifies substantial ATP expenditure. The effects on slow adaptation of PI4K inhibitors suggest that  $\text{PIP}_2$  is normally part of the adaptation motor complex, perhaps responsible in part for localizing Myo1c to membranes. We show here that Myo1c has an anionic phospholipid binding domain in the IQ domains, which also binds calmodulin; this result supports the conclusions of Tang et al. (2002), who showed that  $\text{Ca}^{2+}$  treatment dramatically slows Myo1c dissociation from PS vesicles. After  $\text{Ca}^{2+}$  levels are elevated and calmodulin dissociates from one or two IQ domains, Myo1c will have two separate lipid binding domains exposed, permitting a very strong interaction with anionic phospholipids. The IQ-phospholipid interaction should become insensitive to moderate changes in  $\text{Ca}^{2+}$  after calmodulin dissociates, however, so subsequent  $\text{Ca}^{2+}$  entry during transduction should not affect Myo1c-membrane interactions.

This mechanism could explain recruitment of Myo1c near sites of  $\text{Ca}^{2+}$  entry, such as transduction channels;

only there will Ca<sup>2+</sup> be elevated sufficiently to dissociate calmodulin and expose the IQ lipid binding domain. Once bound to membranes, Myo1c may behave like other polybasic proteins and attract additional PIP<sub>2</sub> molecules to form PIP<sub>2</sub> clusters (McLaughlin et al., 2002). Similar clusters in other cell types resist detergent extraction, as does a subpopulation of PIP<sub>2</sub> in hair bundles, notably at stereocilia tips (Figure 1). Clustered PIP<sub>2</sub> can be much less dynamic than phospholipids are ordinarily thought to be (Wagner and Tamm, 2001). Although concentration of charged lipids by Myo1c might seem to be energetically unfavorable, Myo1c can cluster as many as 50 PS molecules (Tang et al., 2002).

Our data do not conclusively determine whether PIP<sub>2</sub> is required for the integrity of the adaptation motor complex, however. Myo1c receptors at stereocilia tips (Gillespie and Cyr, 2002), which could correspond to adaptation motor complexes, are not affected by PAO treatment (J.-B. Shin, K. Nusser, and P.G.G., unpublished data). Myo1c binds well to membranes containing PS or PIP<sub>2</sub>, suggesting that the identity of anionic phospholipid may not dictate membrane localization. The presence of both PIP<sub>2</sub> and PS in hair bundles, as well as the likely presence of other anionic phospholipids, suggests instead that PIP<sub>2</sub> levels modulate the activity of Myo1c rather than control its assembly into the adaptation motor complex.

#### Adaptation Requires PIP<sub>2</sub>

PIP<sub>2</sub> depletion decreases the rate of adaptation of both fast and slow adaptation. How PIP<sub>2</sub> quantitatively affects the amplitude and kinetics of fast adaptation is not clear, however, because our stimulator slowed the transduction channel kinetics over the timescale of fast adaptation. The 5-fold decrease in adaptation rate that we observed should be a lower limit on the effect of PIP<sub>2</sub>, however, as the distortion due to the stimulator will decrease as the time constant for fast adaptation increases. Because the mechanism of fast adaptation has yet to be established, how PIP<sub>2</sub> depletion affects this process is unclear. Interestingly, although diC8-PIP<sub>2</sub> prevented the increase in resting P<sub>o</sub> elicited by PAO, it did not prevent the slowing of fast adaptation kinetics. This result suggested that diC8-PIP<sub>2</sub> supported slow but not fast adaptation.

Depleting PIP<sub>2</sub> also decreased slipping and climbing rates for slow adaptation; these effects were qualitatively similar to the effects on adaptation of reducing Ca<sup>2+</sup> (Crawford et al., 1991; Assad and Corey, 1992). Because PIP<sub>2</sub> has a 3<sup>-</sup> to 4<sup>-</sup> charge at physiological pH, depletion of this lipid might have decreased the negative surface potential of the plasma membrane (McLaughlin, 1989), decreasing Ca<sup>2+</sup> in the immediate environment of the Ca<sup>2+</sup> sensor for slow adaptation. A prerequisite for this model is that the Myo1c Ca<sup>2+</sup> sensor, presumed to be calmodulin bound to IQ1 (Zhu et al., 1998), must be within the Debye length (1–2 nm) of the membrane. A function of the IQ domain lipid binding site may therefore be to bring the Myo1c Ca<sup>2+</sup> sensor close to the membrane, increasing the Ca<sup>2+</sup> concentration that is detected at the sensor (Figure 7). PIP<sub>2</sub> binding to Myo1c IQ domains could therefore both anchor the motor to a specific site in the cell and increase its apparent sensitivity to Ca<sup>2+</sup>.

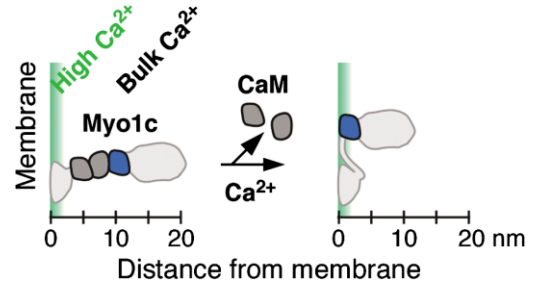


Figure 7. Hypothetical Role of PIP<sub>2</sub> in Regulating Slow Adaptation through Myo1c-Membrane Interaction

(Left) Myo1c with three calmodulins interacts with membranes through its tail. (Right) After calmodulins dissociate, revealing the IQ lipid binding site, the calmodulin bound to IQ1 will be brought closer to the membrane where high surface potential could elevate Ca<sup>2+</sup>. With two binding sites for membranes, Myo1c will also be bound more tightly.

Alternatively, PIP<sub>2</sub> may act to decrease the number of Myo1c molecules in the adaptation motor complex; with fewer myosin molecules, adaptation would be faster and the resting force—and hence resting P<sub>o</sub>—would be lower (Gillespie and Cyr, 2004). This model would imply, however, that PIP<sub>2</sub>-Myo1c complexes do not integrate into the adaptation motor complex.

An important question is whether hair cells vary their PIP<sub>2</sub> levels in order to modulate adaptation kinetics or whether the hair cell simply requires PIP<sub>2</sub> for normal adaptation. Although we found no evidence for phospholipase C $\beta$  regulation of PIP<sub>2</sub>, polyphosphatidylinositol flux in hair cells apparently is high; because of this, a modest increase in the concentration, activity, or localization of PIP<sub>2</sub> synthetic or degradative enzymes could have a profound effect on the steady-state concentration of the lipid. Indeed, we were surprised to find high bundle levels of PIP<sub>2</sub> in extra-atriolar hair cells of the utricle, despite high levels of Ptpqrq; although a catalytically inactive form of Ptpqrq might be present in these bundles, it is also possible that the enzymes that synthesize PIP<sub>2</sub> are present at substantially higher levels than in other hair bundles. Indeed, the dynamics of PIP<sub>2</sub> turnover, rather than the steady-state concentration, might be more important for regulating adaptation and transduction.

Although PIP<sub>2</sub> also stimulates PMCA (Choquette et al., 1984), activation of Ca<sup>2+</sup> pumping cannot fully explain our results. Depletion of PIP<sub>2</sub> should lead to decreased pumping activity and to an elevated Ca<sup>2+</sup> level; increased Ca<sup>2+</sup> might decrease the amplitude of fast or slow adaptation but should increase its kinetics, opposite of our principal result.

#### Transduction Requires PIP<sub>2</sub>

PIP<sub>2</sub> synthesis inhibitors decreased the total amplitude of the transduction current. Dialysis with diC8-PIP<sub>2</sub> slowed the loss of transduction elicited by PAO, suggesting that the effect of PAO on transduction current was due to PIP<sub>2</sub> depletion. These results suggest that, as with several other channels (Hilgemann et al., 2001), the transduction channel requires PIP<sub>2</sub> for activity. Because transduction persisted in the absence of immuno-

cytochemically detectable PIP<sub>2</sub>, any PIP<sub>2</sub> pool associated with the channel must not exchange rapidly with the bulk PIP<sub>2</sub> pool.

While the precise mechanisms by which PIP<sub>2</sub> exerts its effects on adaptation and transduction remain to be resolved, our results show that this phospholipid plays an important role in regulating the function, and perhaps the structure, of the adaptation motor and transduction channel. Determination of the static phospholipid composition of stereocilia membranes and corresponding phospholipid dynamics may well reveal further dimensions of regulation of mechanotransduction by hair cells.

## Experimental Procedures

### Preparation

Experiments were performed on epithelial or dissociated cell preparations of hair cells from the saccular and utricular maculae of bullfrogs (*Rana catesbeiana*) or leopard frogs (*Rana pipiens*). For the epithelial preparation, frogs were double pithed and decapitated, and organs were dissected in frog standard saline (110 mM NaCl, 2 mM KCl, 4 mM CaCl<sub>2</sub>, 2 mM MgCl<sub>2</sub>, 3 mM D-glucose, and 10 mM HEPES at pH 7.25); otolithic membranes were manually removed without protease treatment. For hair cell isolation, inner ears were dissected in low-Ca saline (100 μM CaCl<sub>2</sub>). After removal of the tissue overlying the vestibular nerve, the ear was incubated for 15 min in the low-Ca saline with 1 mM EGTA. The saccular macula was then dissected and digested for ~20 min with protease type XXIV (Sigma, St. Louis, MO) at 65 μg/ml and for 5 min with 100 μg/ml deoxyribonuclease I (Worthington, Lakewood, NJ) and 1 mg/ml bovine serum albumin. In a recording chamber, the otolithic membrane was peeled away, and hair cells were teased from the epithelium with an eyelash. After isolation, hair cells were allowed to settle onto a concanavalin A (Worthington)-coated coverslip at the chamber's bottom.

### Cell Labeling

Epithelial tissues or isolated hair cells were fixed in 2.25% formaldehyde and 0.75% glutaraldehyde in PBS (137 mM NaCl, 2.7 mM KCl, 4.3 mM Na<sub>2</sub>HPO<sub>4</sub>, and 1.4 mM KH<sub>2</sub>PO<sub>4</sub> at pH 7.3) for 30 min and washed in PBS. Formaldehyde (16% stock solution) and glutaraldehyde (8% stock solution) were obtained from Electron Microscopy Sciences (Fort Washington, PA). If necessary, tissues or cells were permeabilized with 0.2% saponin in PBS for 10 min and washed three times with PBS. Tissues or cells were blocked for 40 min in blocking solution (PBS, 3% donkey serum, and 10 mg/ml bovine serum albumin). Epithelial tissues and isolated hair cells were incubated overnight (up to 36 hr for whole-mount tissues) at 4°C with 2 μg/ml primary antibody (anti-PIP<sub>2</sub> mouse IgM monoclonal [Molecular Probes, Eugene, OR] or anti-PIP<sub>2</sub> mouse IgG monoclonal [gift from Dr. Fukami]) in blocking solution, washed three times for 10 min in PBS, and then incubated with a secondary antibody (7.5 μg/ml Cy5-conjugated donkey anti-mouse IgM or 7.5 μg/ml Cy3-conjugated donkey anti-mouse IgG; Jackson ImmunoResearch Laboratories, West Grove, PA) and 0.25 μM FITC-phalloidin (Sigma) in the blocking solution for 2–3 hr at room temperature. Tissues or cells were washed three times for 10 min in PBS, mounted with Vectashield (Vector, Burlingame, CA), and viewed with a Plan Apo-chromat 60× or 100× (each 1.40 NA) oil objectives on a Nikon TE 300 inverted microscope with a Bio-Rad MRC 1024 confocal imaging system (Hercules, CA).

For immunogold electron microscopy, saccular epithelia with intact otolithic membranes were labeled through the anti-PIP<sub>2</sub> antibody stage as above. After washing, saccules were then incubated with 1:10 goat anti-mouse IgG conjugated with 5 nm gold (British BioCell International, Cardiff, Wales, UK). Tissues were postfixed with 2.5% glutaraldehyde in 0.1 M sodium cacodylate (pH 7.2), washed, and stained with 1% osmium tetroxide. Samples were dehydrated through an ethanol series, embedded in LR White resin (Ted Pella), and incubated overnight at 60°C. Sections on grids were

stained with uranyl acetate and lead citrate and viewed with a Philips Morgagni transmission electron microscope.

A rabbit serum was raised to the recombinant intracellular domain of chicken Ptp<sub>rq</sub> (a fragment corresponding to amino acids 2016–2302 of the rat sequence, GenBank AF063249), and the antibodies were affinity purified using the same fragment covalently coupled to Sepharose 4B. Affinity-purified antibodies to the recombinant intracellular domain of rat Ptp<sub>rq</sub> (Seifert et al., 2003) were a kind gift from Dr. Dan Bowen-Pope (University of Washington, Seattle). Both antibodies gave identical staining patterns with frog hair cells.

For labeling PS, hair cells were fixed as for PIP<sub>2</sub> staining. Some cells were permeabilized for 10 min with 0.1% saponin. Cells were incubated for 1 hr with FITC-annexin V (Roche), washed, and visualized with confocal microscopy.

### Whole-Cell Recording

Hair bundles were mechanically stimulated with a fire-polished glass pipette coupled to the kinociliary bulb with gentle suction. Mechanical stimuli were elicited with a one-dimensional piezoelectric bimorph stimulator with a 10%–90% rise time below 2 ms. Patch pipettes (3–5 MΩ) were filled with an internal solution (85 mM CsCl, 3 mM MgCl<sub>2</sub>, 2 mM Na<sub>2</sub>ATP, 1 mM EGTA, and 5 mM HEPES at pH 7.3). The series resistance, which was monitored throughout the experiments, ranged from 10 to 18 MΩ. Transduction currents were recorded from hair cells that were voltage clamped at –60 mV using an Axopatch 200A amplifier and pCLAMP software (Axon Instruments, Foster City, CA); currents were digitized and stored on a computer disk for offline analysis. Displacements ranged in amplitude from –400 to 800 nm with an interval of 100 nm. Transduction currents were low-pass filtered at 2 kHz and digitized at 5 kHz; each record represents the average of three stimulus presentations. All experiments were performed at room temperature (22°C–24°C). Where appropriate, values are presented as mean ± SE.

### Extracting Fast and Slow Adaptation Rates

We used the inferred shift method (Shepherd and Corey, 1994) to determine the adaptive shift of the I(X) curve at each point during adaptation. An initial I(X) curve was extracted from the peak transduction currents for a family of deflections and fit with a three-state Boltzmann relation. A *Mathematica 4.0* program (available on request) was used to solve the following Boltzmann equation (Shepherd and Corey, 1994) for X<sub>c</sub>, the adaptive shift of the I(X) curve at a given time:

$$I = I_{\text{closed}} - \frac{I_{\text{max}}}{(1 + e^{(a_2(p_2 - (X - X_c)))}) \cdot (1 + e^{(a_1(p_1 - (X - X_c)))})} \quad (1)$$

where a<sub>1</sub>, p<sub>1</sub>, a<sub>2</sub>, and p<sub>2</sub> are constants derived from the fit to the initial I(X) curve, X is the static deflection, I is the transduction current at any given time, I<sub>closed</sub> is the membrane current when all transduction channels are closed, and I<sub>max</sub> is the maximum current. Because the fit is less accurate at either end of the I(X) curve, we eliminated points derived from regions where its slope was less than 5% of the maximum slope.

A single data set included transduction currents in response to positive steps of 100–800 nm. We simultaneously fit the entire data set with eight equations of the following form:

$$X_c(n) = a_{n1} \cdot e^{-t/\tau_{\text{fast}}} + a_{n2} \cdot e^{-t/\tau_{\text{slow}}} \quad (2)$$

where X<sub>c</sub>(n) is the adaptive shift for a displacement of size n, a<sub>n1</sub> and a<sub>n2</sub> are the amplitudes for fast and slow adaptation for that displacement, and τ<sub>fast</sub> and τ<sub>slow</sub> are the two global time constants for fast and slow adaptation. The initial rates of adaptation for a given displacement were a<sub>n1</sub>/τ<sub>fast</sub> and a<sub>n2</sub>/τ<sub>slow</sub>. Note that this differs from previous analyses; here, the time constants for fast and slow adaptation were assumed to be the same for all stimuli, with varying amplitudes.

Time constants for adaptation to negative deflections were determined using the method of Holt et al. (2002). When the bundle was returned to rest after such a displacement, the overshoot (or tail) current reflected the amount of adaptation that took place during the stimulus. The amplitude of the overshoot current was compared to an I(X) relation obtained immediately prior; equivalent displace-

ments for each overshoot current were plotted relative to stimulus duration, and the data were fit with a sum of exponential and linear terms.

#### Transduction Current Simulations

The transduction and adaptation model of Shepherd and Corey (1994) was implemented using a *Mathematica* program (available on request). The model calculates the position of the transduction complex at any point before, during, or after a stimulus with a stiff probe (ixpos); the movement is described by a sum of two exponential functions with relative weighting determined empirically (Figures 5E and 5F) and total movement limited by an extent spring. ixpos is converted into a transduction current with the use of a three-state Boltzmann relation as in equation 1. Parameter values used for before and during PAO treatment are listed in Table 1.

#### Biochemistry

Epitope-tagged (Xpress tag) full-length frog Myo1c and its fragments (T701, residues 701–1028; N123, residues 701–790) were expressed and purified as described (Cyr et al., 2002; Gillespie and Cyr, 2002). Phospholipid vesicles were made by sonication (100 mol% PS vesicles only) or by extrusion through 100 nm pore filters using a Mini-Extruder (Avanti Polar Lipids). For calmodulin release experiments, His<sub>6</sub>-Myo1c was mixed with 100 mol% PS vesicles at varied Ca<sup>2+</sup> concentrations, then unbound His<sub>6</sub>-Myo1c with its calmodulin light chains was removed with Ni<sup>2+</sup>-NTA resin. Remaining free calmodulin, displaced when Myo1c binds PS, was detected by an ELISA assay (Gillespie et al., 1999). PIP strips (Molecular Probes) were blocked with Liquid Block (Amersham), probed with 1 μg/ml recombinant Myo1c or the N123 fragment in the presence or absence of 5 μM calmodulin, and detected with 1:2000 anti-Xpress antibody (Invitrogen) and 1:10,000 HRP-labeled anti-mouse IgG (Jackson ImmunoResearch).

Binding of the N123 fragment of Myo1c to phospholipid vesicles was measured using an adaptation of the solid-phase assay of Fukami et al. (1996). N123 was captured on microtiter plates with an antibody sandwich. Following a 0.5 hr absorption of 0.2 mg/ml donkey anti-mouse IgG (Jackson ImmunoResearch), unreacted binding sites were blocked for 1 hr with 0.5 mg/ml hemoglobin. Anti-Xpress antibody (Invitrogen) at 2 μg/ml in 0.5 mg/ml hemoglobin was added to plate wells for 1 hr, then Xpress-tagged N123 (5 μg/ml) was allowed to bind overnight. Phospholipid vesicles incorporating 10 mol% rhodamine-phosphatidylethanolamine (Avanti), 40 mol% phosphatidylcholine (Avanti), and 50 mol% PS (Avanti) or PIP<sub>2</sub> (Roche) were incubated in plate wells for 1 hr in the presence of varying concentrations of Ca<sup>2+</sup> and calmodulin. Following 3 × 5 min washes, fluorescence was measured using microplate fluorometer.

#### Acknowledgments

We thank Dr. P. Mayinger and members of the Gillespie lab for constructive criticism of the manuscript. Dr. J. Cyr (West Virginia University) and Dr. T. Yoshioka (Waseda University) participated in helpful discussions of the project. Y. Kim carried out preliminary lipid-binding experiments; K. Nusser and W. Zhao provided excellent technical support. Immunogold electron microscopy was carried out with M. Webb of the OHSU Electron Microscopy Core. We thank Dr. K. Fukami of Tokyo University for the gift of the KT10 anti-PIP<sub>2</sub> antibody. Supported by NIH grants R01 DC002387, R01 DC004571, and P30 DC005983 (to P.G.G.); and Wellcome Trust grant 057410/Z/99/Z (to G.P.R.).

Received: June 18, 2004

Revised: August 17, 2004

Accepted: August 24, 2004

Published: October 13, 2004

#### References

Arcaro, A., and Wymann, M.P. (1993). Wortmannin is a potent phosphatidylinositol 3-kinase inhibitor: the role of phosphatidylinositol 3,4,5-trisphosphate in neutrophil responses. *Biochem. J.* 296, 297–301.

Assad, J.A., and Corey, D.P. (1992). An active motor model for adaptation by vertebrate hair cells. *J. Neurosci.* 12, 3291–3309.

Assad, J.A., Shepherd, G.M.G., and Corey, D.P. (1991). Tip-link integrity and mechanical transduction in vertebrate hair cells. *Neuron* 7, 985–994.

Augert, G., Blackmore, P.F., and Exton, J.H. (1989). Changes in the concentration and fatty acid composition of phosphoinositides induced by hormones in hepatocytes. *J. Biol. Chem.* 264, 2574–2580.

Balla, T. (1998). Phosphatidylinositol 4-kinases. *Biochim. Biophys. Acta* 1436, 69–85.

Balla, T., Bondeva, T., and Varnai, P. (2000). How accurately can we image inositol lipids in living cells? *Trends Pharmacol. Sci.* 21, 238–241.

Choquette, D., Hakim, G., Filoteo, A.G., Plishker, G.A., Bostwick, J.R., and Penniston, J.T. (1984). Regulation of plasma membrane Ca<sup>2+</sup> ATPases by lipids of the phosphatidylinositol cycle. *Biochem. Biophys. Res. Commun.* 125, 908–915.

Cochet, C., and Chambaz, E.M. (1986). Catalytic properties of a purified phosphatidylinositol-4-phosphate kinase from rat brain. *Biochem. J.* 237, 25–31.

Crawford, A.C., Evans, M.G., and Fettiplace, R. (1991). The actions of calcium on the mechano-electrical transducer current of turtle hair cells. *J. Physiol.* 434, 369–398.

Cyr, J.L., Dumont, R.A., and Gillespie, P.G. (2002). Myosin-1c interacts with hair-cell receptors through its calmodulin-binding IQ domains. *J. Neurosci.* 22, 2487–2495.

Eatock, R.A., Corey, D.P., and Hudspeth, A.J. (1987). Adaptation of mechano-electrical transduction in hair cells of the bullfrog's sacculus. *J. Neurosci.* 7, 2821–2836.

Edidin, M. (2003). The state of lipid rafts: from model membranes to cells. *Annu. Rev. Biophys. Biomol. Struct.* 32, 257–283.

Fettiplace, R., and Ricci, A.J. (2003). Adaptation in auditory hair cells. *Curr. Opin. Neurobiol.* 13, 446–451.

Fukami, K., Matsuoka, K., Nakanishi, O., Yamakawa, A., Kawai, S., and Takenawa, T. (1988). Antibody to phosphatidylinositol 4,5-bisphosphate inhibits oncogene-induced mitogenesis. *Proc. Natl. Acad. Sci. USA* 85, 9057–9061.

Fukami, K., Sawada, N., Endo, T., and Takenawa, T. (1996). Identification of a phosphatidylinositol 4,5-bisphosphate-binding site in chicken skeletal muscle α-actinin. *J. Biol. Chem.* 271, 2646–2650.

Gerke, V., and Moss, S.E. (2002). Annexins: from structure to function. *Physiol. Rev.* 82, 331–371.

Gillespie, P.G., and Cyr, J.L. (2002). Calmodulin binding to recombinant myosin-1c and myosin-1c IQ peptides. *BMC Biochem.* 3, 31.

Gillespie, P.G., and Cyr, J.L. (2004). Myosin-1c, the hair cell's adaptation motor. *Annu. Rev. Physiol.* 66, 521–545.

Gillespie, P.G., Gillespie, S.K., Mercer, J.A., Shah, K., and Shokat, K.M. (1999). Engineering of the myosin-Iβ nucleotide-binding pocket to create selective sensitivity to N<sup>6</sup>-modified ADP analogs. *J. Biol. Chem.* 274, 31373–31381.

Goodyear, R., and Richardson, G. (1992). Distribution of the 275 kD hair cell antigen and cell surface specialisations on auditory and vestibular hair bundles in the chicken inner ear. *J. Comp. Neurol.* 325, 243–256.

Goodyear, R.J., Legan, P.K., Wright, M.B., Marcotti, W., Oganessian, A., Coats, S.A., Booth, C.J., Kros, C.J., Seifert, R.A., Bowen-Pope, D.F., and Richardson, G.P. (2003). A receptor-like inositol lipid phosphatase is required for the maturation of developing cochlear hair bundles. *J. Neurosci.* 23, 9208–9219.

Hannah, M.J., Weiss, U., and Huttner, W.B. (1998). Differential extraction of proteins from paraformaldehyde-fixed cells: lessons from synaptophysin and other membrane proteins. *Methods* 16, 170–181.

Hilgemann, D.W., Feng, S., and Nasuhoglu, C. (2001). The complex and intriguing lives of PIP<sub>2</sub> with ion channels and transporters. *Sci. STKE* 2001, RE19.

Hinners, I., Moschner, J., Nolte, N., and Hille-Rehfeld, A. (1999). The

- orientation of membrane proteins determined in situ by immunofluorescence staining. *Anal. Biochem.* 276, 1–7.
- Holt, J.R., Gillespie, S.K., Provance, D.W., Shah, K., Shokat, K.M., Corey, D.P., Mercer, J.A., and Gillespie, P.G. (2002). A chemical-genetic strategy implicates myosin-1c in adaptation by hair cells. *Cell* 108, 371–381.
- Kachar, B., Parakkal, M., Kurc, M., Zhao, Y., and Gillespie, P.G. (2000). High-resolution structure of hair-cell tip links. *Proc. Natl. Acad. Sci. USA* 97, 13336–13341.
- Kroese, A.B., Das, A., and Hudspeth, A.J. (1989). Blockage of the transduction channels of hair cells in the bullfrog's sacculus by aminoglycoside antibiotics. *Hear. Res.* 37, 203–217.
- Lemmon, M.A. (2003). Phosphoinositide recognition domains. *Traffic* 4, 201–213.
- Lumpkin, E.A., and Hudspeth, A.J. (1998). Regulation of free  $Ca^{2+}$  concentration in hair-cell stereocilia. *J. Neurosci.* 18, 6300–6318.
- McLaughlin, S. (1989). The electrostatic properties of membranes. *Annu. Rev. Biophys. Chem.* 18, 113–136.
- McLaughlin, S., Wang, J., Gambhir, A., and Murray, D. (2002).  $PIP_2$  and proteins: interactions, organization, and information flow. *Annu. Rev. Biophys. Biomol. Struct.* 31, 151–175.
- Oganesian, A., Poot, M., Daum, G., Coats, S.A., Wright, M.B., Seifert, R.A., and Bowen-Pope, D.F. (2003). Protein tyrosine phosphatase RQ is a phosphatidylinositol phosphatase that can regulate cell survival and proliferation. *Proc. Natl. Acad. Sci. USA* 100, 7563–7568.
- Ozaki, S., DeWald, D.B., Shope, J.C., Chen, J., and Prestwich, G.D. (2000). Intracellular delivery of phosphoinositides and inositol phosphates using polyamine carriers. *Proc. Natl. Acad. Sci. USA* 97, 11286–11291.
- Pickles, J.O., Comis, S.D., and Osborne, M.P. (1984). Cross-links between stereocilia in the guinea pig organ of Corti, and their possible relation to sensory transduction. *Hear. Res.* 15, 103–112.
- Rohacs, T., Chen, J., Prestwich, G.D., and Logothetis, D.E. (1999). Distinct specificities of inwardly rectifying  $K^+$  channels for phosphoinositides. *J. Biol. Chem.* 274, 36065–36072.
- Rzadzinska, A.K., Schneider, M.E., Davies, C., Riordan, G.P., and Kachar, B. (2004). An actin molecular treadmill and myosins maintain stereocilia functional architecture and self-renewal. *J. Cell Biol.* 164, 887–897.
- Schaefer, T., Wiedemann, C., Gitler, C., and Burger, M.M. (1994). Effects of arsenicals on the secretory process in chromaffin cells. *Ann. N Y Acad. Sci.* 710, 356–367.
- Seifert, R.A., Coats, S.A., Oganesian, A., Wright, M.B., Dishmon, M., Booth, C.J., Johnson, R.J., Alpers, C.E., and Bowen-Pope, D.F. (2003). PTPRQ is a novel phosphatidylinositol phosphatase that can be expressed as a cytoplasmic protein or as a subcellularly localized receptor-like protein. *Exp. Cell Res.* 287, 374–386.
- Shepherd, G.M.G., and Corey, D.P. (1994). The extent of adaptation in bullfrog saccular hair cells. *J. Neurosci.* 14, 6217–6229.
- Swanlung-Collins, H., and Collins, J.H. (1992). Phosphorylation of brush border myosin I by protein kinase C is regulated by  $Ca^{2+}$ -stimulated binding of myosin I to phosphatidylserine concerted with calmodulin dissociation. *J. Biol. Chem.* 267, 3445–3454.
- Tachibana, M., Morioka, H., Machino, M., Oshima, W., Mizukoshi, F., Mizukoshi, O., and Yoshioka, T. (1984). Localization of triphosphoinositide in the cochlea. An electronmicroscopic immunocytochemical study. *Histochemistry* 81, 157–160.
- Tang, N., Lin, T., and Ostap, E.M. (2002). Dynamics of myo1c (myosin- $\beta$ ) lipid binding and dissociation. *J. Biol. Chem.* 277, 42763–42768.
- Thomas, C.L., Steel, J., Prestwich, G.D., and Schiavo, G. (1999). Generation of phosphatidylinositol-specific antibodies and their characterization. *Biochem. Soc. Trans.* 27, 648–652.
- Varnai, P., and Balla, T. (1998). Visualization of phosphoinositides that bind pleckstrin homology domains: calcium- and agonist-induced dynamic changes and relationship to myo-[ $^3H$ ]inositol-labeled phosphoinositide pools. *J. Cell Biol.* 143, 501–510.
- Vollrath, M.A., and Eatock, R.A. (2003). Time course and extent of mechanotransducer adaptation in mouse utricular hair cells: comparison with frog saccular hair cells. *J. Neurophysiol.* 90, 2676–2689.
- Wagner, M.L., and Tamm, L.K. (2001). Reconstituted syntaxin1A/SNAP25 interacts with negatively charged lipids as measured by lateral diffusion in planar supported bilayers. *Biophys. J.* 81, 266–275.
- Wang, B.M., Weiner, N.D., Takada, A., and Schacht, J. (1984). Characterization of aminoglycoside-lipid interactions and development of a refined model for ototoxicity testing. *Biochem. Pharmacol.* 33, 3257–3262.
- Wiedemann, C., Schaefer, T., and Burger, M.M. (1996). Chromaffin granule-associated phosphatidylinositol 4-kinase activity is required for stimulated secretion. *EMBO J.* 15, 2094–2101.
- Williamson, P., and Schlegel, R.A. (1994). Back and forth: the regulation and function of transbilayer phospholipid movement in eukaryotic cells. *Mol. Membr. Biol.* 11, 199–216.
- Wu, Y.C., Ricci, A.J., and Fettiplace, R. (1999). Two components of transducer adaptation in auditory hair cells. *J. Neurophysiol.* 82, 2171–2181.
- Yamoah, E.N., Lumpkin, E.A., Dumont, R.A., Smith, P.J., Hudspeth, A.J., and Gillespie, P.G. (1998). Plasma membrane  $Ca^{2+}$ -ATPase extrudes  $Ca^{2+}$  from hair cell stereocilia. *J. Neurosci.* 18, 610–624.
- Yin, H.L., and Janmey, P.A. (2003). Phosphoinositide regulation of the actin cytoskeleton. *Annu. Rev. Physiol.* 65, 761–789.
- Zhu, T., Sata, M., and Ikebe, M. (1996). Functional expression of mammalian myosin I $\beta$ : analysis of its motor activity. *Biochemistry* 35, 513–522.
- Zhu, T., Beckingham, K., and Ikebe, M. (1998). High affinity  $Ca^{2+}$  binding sites of calmodulin are critical for the regulation of myosin I $\beta$  motor function. *J. Biol. Chem.* 273, 20481–20486.